ASTRONOMY & ASTROPHYSICS
SUPPLEMENT SERIES

AUGUST **1996**, PAGE 263

*Astron. Astrophys. Suppl. Ser.* **118,** 263-275 (1996)

# Results of the ESO-SEST Key Programme: CO in the Magellanic Clouds. V. Further CO observations of the Small Magellanic Cloud⋆

M. Rubio[1], J. Lequeux[2,3], F. Boulanger[2,4], R.S. Booth[5], G. Garay[1], Th. de Graauw[6], F.P. Israel[7], L.E.B. Johansson[5,10], M.L. Kutner[8,9] and L.–Å. Nyman[5,10]

[1] Departamento de Astronomía , Universidad de Chile, Casilla 36-D, Santiago, Chile
[2] Radioastronomie, Ecole Normale Superieure, 24 Rue Lhomond, 75231 Paris Cedex 05, France
[3] DEMIRM, Observatoire de Paris, 61 Av. de l'Observatoire, 75014 Paris, France
[4] Institut d'Astrophysique Spatiale, Bat. 120, Université de Paris-XI, 91045 Orsay cedex, France
[5] Onsala Space Observatory, S-43900 Onsala, Sweden
[6] Laboratorium voor Ruimteonderzoek, SRON, Postbus 800, NL-9700 AV Groningen, The Netherlands
[7] Sterrewacht, Postbus 9513, NL-2300 Leiden, The Netherlands
[8] Department of Physics, Rensselaer Polytechnic Institute, Troy, NY 12180, U.S.A.
[9] NRAO, 949 N. Cherry Av., Campus Building 65, Tucson , Arizona 85721-0655, U.S.A.
[10] European Southern Observatory, Casilla 19001, Santiago 19, Chile

Received September 9, 1995; accepted January 3, 1996

**Abstract.** — We present further results of fully-sampled observations in the $J = 1 \rightarrow 0$ and $J = 2 \rightarrow 1$ rotational transitions of $^{12}$CO and $^{13}$CO, obtained with the SEST telescope at 43″ or 22″ resolution, toward the Small Magellanic Cloud. These observations concern six molecular clouds with a variety of physical conditions. Maps in the $^{12}$CO(1→0), $^{12}$CO(2→1), and in some cases of $^{13}$CO(1→0) lines are presented, as well as profiles of the four lines at the peak positions convolved to the same angular resolution of 43″. The line ratio results are interpreted in Paper IV of this series (Lequeux et al. 1994).

**Key words:** Magellanic Clouds — galaxies: ISM — interstellar medium: molecules — interstellar medium: clouds — radio lines: galaxies

## 1. Introduction

The ESO SEST Key programme was established to investigate the properties of the molecular gas in the Magellanic Clouds. The motivation for this Key Programme can be found in Israel et al. (1993: Paper I), the results being presented as a series of publications. Several papers in this series (Rubio et al. 1993: Paper II; Rubio et al. 1993: Paper III; and Lequeux et al. 1994: Paper IV) have presented and discussed observations of molecular clouds in the Small Molecular Cloud (SMC) in the $J = 1 \rightarrow 0$ and $J = 2 \rightarrow 1$ rotational transitions of the $^{12}$CO and $^{13}$CO molecules. The main conclusion is that molecular clouds in the SMC have properties different from those of Galactic molecular clouds. The differences can be explained by the combined effects of a higher UV radiation field and of a lower abundance of heavy elements and of dust, while the density structure of the clouds is not necessarily different from that of their Galactic counterparts (Papers III and IV).

To determine the physical properties of molecular clouds it is essential to have data in different molecular species and transitions (cf. Castets et al. 1990). In this paper we present the data from observations in the $^{12}$CO(1→0), $^{12}$CO(2→1), $^{13}$CO(2→1) and $^{13}$CO(1→0) lines toward six molecular clouds: LIRS 36, LIRS 49 (both designated from the name of the associated infrared source, Schwering & Israel 1989), SMC-B1#1 (Paper II), N66 and N88 (associated with the two brightest HII regions in the SMC, Henize 1956) and Hodge 15 (named after the associated dark cloud; Hodge 1984). These clouds were selected as they cover a wide range of ambient conditions in the SMC. Only two of them, SMCB1#1 and Hodge 15 were observed as part of the CO mapping of the SMC-B1 and SMC-B2 regions in the SMC (Paper II). In

*Send offprint requests to*: J. Lequeux
⋆based on results collected at the European Southern Observatory, La Silla, Chile

particular, we present line profiles at the peak positions convolved to the same effective angular resolution (43″) toward five clouds. The data of LIRS 49 was presented in Paper II. The line ratios derived from these data have been used in Paper IV to discuss the physical properties of these clouds. We also present fully-sampled maps of the emission in the $^{12}$CO(1→0) transition, maps in the $^{12}$CO(2→1) transition, and in some cases maps of the $^{13}$CO(1→0) transition. In Sect. 2 we describe the observations and reductions, in Sect. 3 we present the four spectra at the peak position of the five sources, and in Sect. 4 we present the grid of spectra across the sources.

## 2. Observations and reductions

The observations were made during several runs with the Swedish-ESO Submillimeter Telescope (SEST). This radiotelescope is located at La Silla Observatory (Chile) and has a diameter of 15 m. The FWHM beam is 43″ at the frequency of the $J = 1 \rightarrow 0$ line, and 22″ at the frequency of the $J = 2 \rightarrow 1$ line. The backend is an acousto-optical spectrometer with a total bandwidth of 86 MHz and a channel width of 0.043 MHz. This corresponds to a velocity range of 230 km s$^{-1}$ and a velocity resolution of 0.11 km s$^{-1}$ at the frequency of the $^{12}$CO(1→0) line, and to 112 km s$^{-1}$ and 0.056 km s$^{-1}$ at the frequency of the $^{12}$CO(2→1) line. The observations of the $^{12}$CO(1→0) line were done in the frequency-switch mode with a throw of 15 MHz. For the other three lines the observations were made in the position-switching mode, with a reference position far from the known CO emission zones. In general the four lines were observed independently, except for a few observations where data at $^{12}$CO(1→0) and $^{13}$CO(1→0) could be obtained simultaneously. The system temperature varied between 400 and 800 K for $^{12}$CO(1→0) and 900 to 1500 K for $^{12}$CO(2→1). The integration time for the maps was automatically varied in order to secure a uniform noise level, in general 0.1 K per channel at all frequencies. Telescope pointing was done toward the strong SiO maser R Dor. A calibration scan on the strongest lines in the SMC (those of LIRS 49) was always performed at the beginning of the run to check the emission level since pointing on R Dor was possible only at the end of the observations. We estimate the maximum pointing errors as about 5″. The calibration used the usual absorbing chopping wheel method, and observations of blackbodies at two temperatures. The antenna temperature scale was checked sporadically on the cloud OMC1.

The data reduction was performed using the CLASS package. The spectra were reduced with a baseline fit of order 2 or 3 which should introduce little error because of the relative narrowness of the lines. Those obtained in the frequency switch mode were subsequently folded. The data are given either in the antenna temperature scale $T_{\rm A}^*$ (Figs. and Table 1) or in the main-beam scale $T_{\rm mb} = T_{\rm A}^*/\eta$ (Table 2) where $\eta$ is the main beam efficiency. The values of $\eta$ assumed for all observations presented in this paper are 0.70 and 0.60 at 115 and 230 GHz, respectively. These values differ slightly from those of Papers I-III where a different choice of the efficiency at 115 GHz was used. We estimate that the absolute calibrations are accurate to ±15% and, more importantly, that the intensity ratios of the $^{12}$CO(2→1) and $^{12}$CO(1→0) lines are known to within 20%. The ratio of the $^{13}$CO(2→1) and $^{13}$CO(1→0) lines are less well determined because of the poorer signal-to-noise ratios and are accurate to 30% at best. Of course the ratios between the $^{13}$CO(1→0) and the $^{12}$CO(1→0) or between the $^{13}$CO(2→1) and the $^{12}$CO(2→1) line intensities are less dependent on absolute calibration, but the signal-to-noise ratio is poorer for the $^{13}$CO(1→0) lines and therefore the final ratios are known to within 20% with some exceptions.

## 3. Line profiles at the peak positions

Figures 1 to 5 display the profiles of the $J = 1 \rightarrow 0$ and $J = 2 \rightarrow 1$ lines of $^{12}$CO and $^{13}$CO at the peak positions of five clouds. The line profiles of source LIRS 49 can be found in Paper II (their Fig. 7). The spectra have been smoothed (Hanning or boxcar) for presentation, thus the velocity resolution in these figures is about 0.4 km s$^{-1}$ . The abscissae in Figs. 1-5 are LSR velocities and the ordinates are antenna temperatures $T_{\rm A}^*$. Table 1 gives for each cloud the line parameters of the four transitions, obtained from a one component gaussian fit to the line profiles. All profiles refer to the same angular resolution of 43″, which is that of the SEST at 115 GHz. In order to make these profiles at 230 GHz, we made observations on a $3 \times 3$ point grid of $20'' \times 20''$ step centered on the peak position observed at 115 GHz, weighting and adding them in such a way to simulate the 115 GHz beam. This procedure is exact for a point and a uniform source, and only approximate for a somewhat extended source, but the differences with the exact solution is negligible compared to the calibration uncertainties. Table 2 gives for each source the coordinates of the peak position, obtained from the $^{12}$CO(1→0) observations, and the derived ratios of the velocity integrated line intensities, $\int T_{\rm mb} {\rm d}v$. The quantities in Tables 1 and 2 may differ slightly from those given in Papers I to III as we have selected the best data available, redone all the reductions (except for LIRS 49) and included some recent observations.

Based on the closeness to bright HII regions and values of the $^{13}$CO(2→1)/$^{13}$CO(1→0) integrated line intensity ratios, the six clouds under consideration can be grouped, although somewhat subjectively, into three categories: i) the "hot" clouds, N88 and N66, which are close to bright HII regions and have $^{13}$CO(2→1)/$^{13}$CO(1→0) $\geq$ 2 ; ii) the "warm" clouds, LIRS 49 and LIRS 36, which are near to less bright HII regions and have 1 < $^{13}$CO(2→1)/$^{13}$CO(1→0) < 2 ; iii) the "cold" clouds, SMC-B1#1 and Hodge 15, which are far from HII regions

**Table 1.** Line parameters at peak position[a]

| Cloud | $^{12}$CO(1−0) | | | | $^{12}$CO(2−1) | | | |
|---|---|---|---|---|---|---|---|---|
| | $T_A^*$ (K) | $V$ (km s$^{-1}$) | $\Delta v$[b] (km s$^{-1}$) | $\int T_A^* dv$ (K km s$^{-1}$) | $T_A^*$ (K) | $V$ (km s$^{-1}$) | $\Delta v$ (km s$^{-1}$) | $\int T_A^* dv$ (K km s$^{-1}$) |
| LIRS 49 | 1.45 | 114.6±0.1 | 5.2±0.2 | 8.0±0.4 | 1.54 | 114.6±0.1 | 5.4±0.1 | 8.9±0.2 |
| LIRS 36 | 1.77 | 126.1±0.1 | 3.1±0.2 | 5.9±0.3 | 1.35 | 126.3±0.1 | 3.7±0.1 | 5.3±0.1 |
| SMC-B1#1 | 1.01 | 122.3±0.1 | 2.8±0.1 | 3.0±0.1 | 0.62 | 122.2±0.1 | 3.3±0.1 | 3.3±0.1 |
| N66 | 0.45 | 160.6±0.1 | 6.6±0.3 | 3.5±0.1 | 0.58 | 160.1±0.1 | 6.2±0.1 | 3.8±0.1 |
| N88 | 0.47 | 147.8±0.1 | 3.5±0.2 | 1.7±0.1 | 0.39 | 147.7±0.1 | 3.5±0.2 | 1.5±0.1 |
| Hodge15 | 0.63 | 122.0±0.1 | 4.6±0.2 | 3.1±0.1 | 0.66 | 122.2±0.1 | 4.4±0.2 | 3.1±0.1 |
| Cloud | $^{13}$CO(1−0) | | | | $^{13}$CO(2−1) | | | |
| | $T_A^*$ (K) | $V$ (km s$^{-1}$) | $\Delta v$ (km s$^{-1}$) | $\int T_A^* dv$ (K km s$^{-1}$) | $T_A^*$ (K) | $V$ (km s$^{-1}$) | $\Delta v$ (km s$^{-1}$) | $\int T_A^* dv$ (K km s$^{-1}$) |
| LIRS 49 | 0.10 | 114.7±0.1 | 4.9±0.3 | 0.51±0.03 | 0.16 | 114.5±0.2 | 4.2±0.2 | 0.72±0.05 |
| LIRS 36 | 0.21 | 126.1±0.1 | 2.4±0.2 | 0.53±0.03 | 0.24 | 126.0±0.1 | 2.3±0.2 | 0.59±0.05 |
| SMC-B1#1 | 0.11 | 121.9±0.1 | 2.0±0.2 | 0.24±0.03 | 0.11 | 122.2±0.2 | 1.8±0.3 | 0.20±0.03 |
| N66 | 0.07 | 159.7±0.1 | 4.4±0.3 | 0.32±0.05 | 0.09 | 160.5±0.2 | 5.7±0.7 | 0.57±0.05 |
| N88 | 0.05 | 147.3±0.1 | 1.20±0.2 | 0.07±0.01 | 0.09 | 148.4±0.1 | 1.8±0.3 | 0.16±0.03 |
| Hodge15 | 0.12 | 122.4±0.3 | 3.3±0.7 | 0.42±0.07 | 0.09 | 122.3±0.3 | 2.1±0.7 | 0.21±0.06 |

[a] quoted errors are $1\sigma$ errors from gaussian fit
[b] FWHM

**Table 2.** Ratios of integrated line intensities

| Cloud | Peak position | | $\frac{^{12}\text{CO(2-1)}}{^{12}\text{CO}(1-0)}$ | $\frac{^{13}\text{CO(2-1)}}{^{13}\text{CO}(1-0)}$ | $\frac{^{12}\text{CO(1-0)}}{^{13}\text{CO}(1-0)}$ | $\frac{^{12}\text{CO(2-1)}}{^{13}\text{CO}(2-1)}$ |
|---|---|---|---|---|---|---|
| | $\alpha$(1950) | $\delta$(1950) | | | | |
| LIRS 49 | $0^h46^m32^s.9$ | -73° 21' 50" | 1.3[a] | 1.6[b] | 16[a] | 12[a] |
| LIRS 36 | 0 44 51.6 | -73 22 30 | 1.1[a] | 1.3[b] | 11[a] | 9[a] |
| SMC-B1#1 | 0 43 42.4 | -73 35 10 | 0.84[a] | 1.0[b] | 13[a] | 11[a] |
| N66 | 0 57 39.7 | -72 25 16 | 1.3[a] | 2.1[b] | 11[a] | 7[a] |
| N88 | 1 22 54.1 | -73 24 33 | 1.0[a] | 2.7[b] | 25[b] | 9[b] |
| Hodge15 | 0 46 23.0 | -73 39 10 | 1.2[a] | 0.6[c] | 7[b] | 15[c] |

[a] accurate to 20%; [b] accurate to 30%; [c] accurate to 40%

and have $^{13}$CO(2→1)/$^{13}$CO(1→0) ≤ 1. The physics of these clouds has been discussed in Paper IV.

## 4. Grids of line profiles

Grids of the line profiles in the $^{12}$CO(1→0), $^{12}$CO(2→1), and in some cases of $^{13}$CO(1→0) transitions from the six clouds are displayed in Figs. 6 to 11. Most of the $^{12}$CO(2→1) mapping was done centered on the peak position of the $^{12}$CO(1→0) emission (marked in the grid), and do not fully cover the source extent, since these observations were mainly designed to compare them with the $^{12}$CO(1→0) emission at the peak position. We show grids of profiles, rather than contour maps, since they provide a good idea of the signal to noise ratio achieved in the observations and of the extension of the clouds with respect to the beam size. The sampling was done in a $20'' \times 20''$ grid for the $^{12}$CO(1→0) observations and in a $10'' \times 10''$ grid for the $^{12}$CO(2→1), about half the HPBW of the SEST at the respective frequency. The velocity scale is LSR velocity, the velocity resolution is 0.11 km s$^{-1}$ for the $^{12}$CO(1→0) profiles and 0.06 km s$^{-1}$ for the $^{12}$CO(2→1) profiles, and the intensity scale is antenna temperature, $T_A^*$. For each map the most convenient velocity range was used in order to show the velocity width of the emission.

*Acknowledgements.* We thank the SEST staff and team for their continuous cooperation. M.R. wishes to acknowledge support from FONDECYT (Chile) trough grant 1930928. SEST is operated jointly by ESO and the Swedish National Facility for Radioastronomy.

## References

Castets A., Duvert G., Dutrey A., et al., 1990, A&A 234, 469
Henize K., 1956, ApJS 2, 315
Hodge P., 1974, PASP 86, 263
Israel F.P., Johansson L.E.B., Lequeux J., et al., 1993, A&A 276, 25 (Paper I)
Lequeux J., Le Bourlot J., Pineau des Forets G., et al., 1994, A&A 292, 371 (Paper IV)
Rubio M., Lequeux J., Boulanger F., et al., 1993, A&A 271, 1 (Paper II)
Rubio M., Lequeux J., Boulanger F., 1993, A&A 271, 9 (Paper III)
Schwering P.B.W., Israel F.P., 1989, A&AS 79, 79

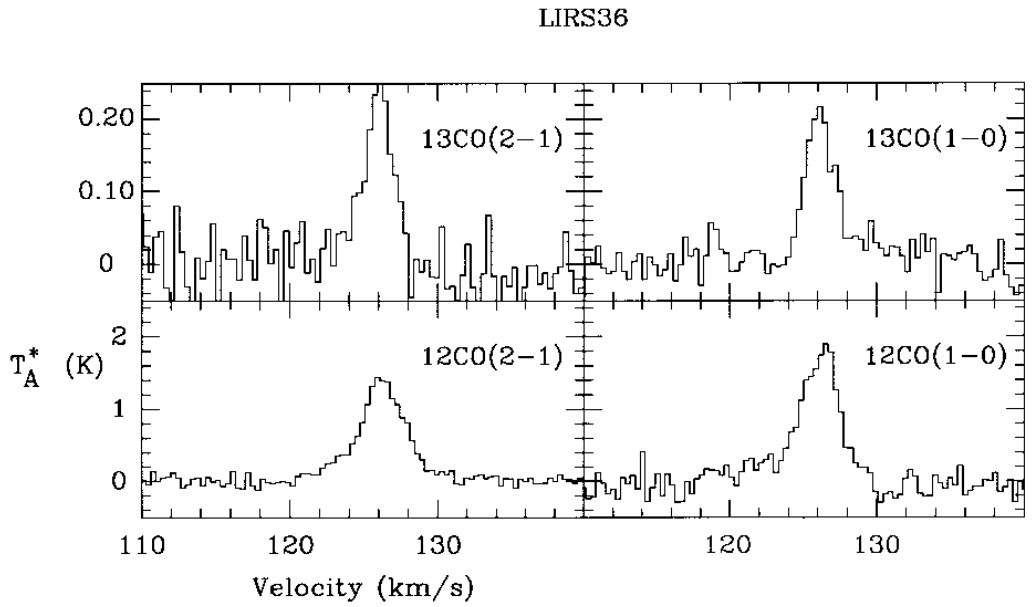


**Fig. 1.** Spectra in the $^{12}$CO(1→0), $^{12}$CO(2→1), $^{13}$CO(1→0), $^{13}$CO(2→1) lines at the peak position, $\alpha = 0^{\rm h}44^{\rm m}51\overset{\prime\prime}{.}6$, $\delta = -73^\circ 22' 30''$ (1950.0), of the molecular cloud LIRS 36. The $J = 2 \rightarrow 1$ data have been smoothed to the same angular resolution of the $J = 1 \rightarrow 0$ data ($43''$). The axis are velocity in $V_{\rm lsr}$ and temperature in $T_{\rm A}^*$

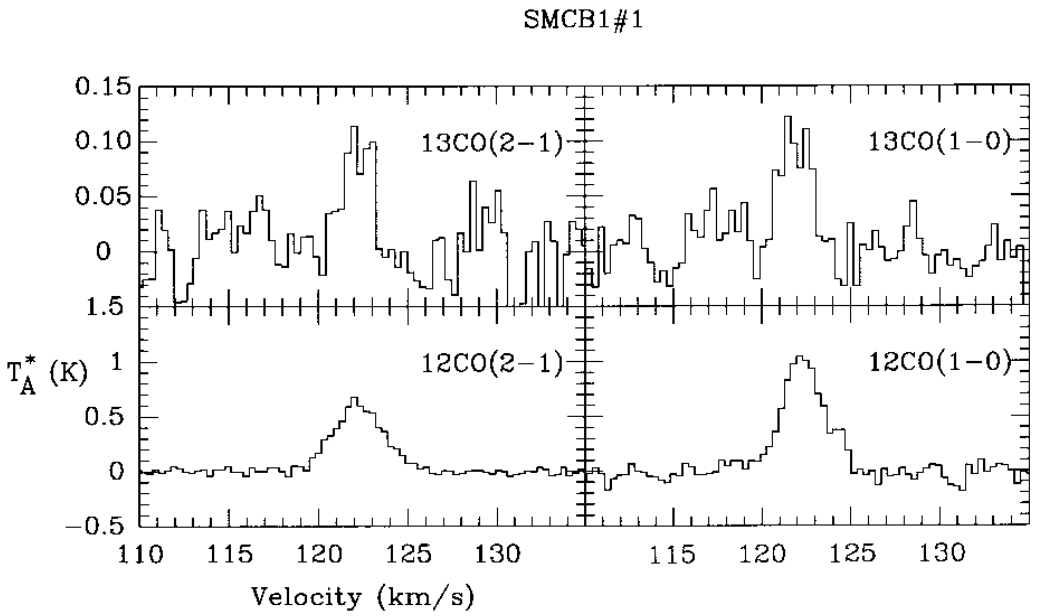


**Fig. 2.** Spectra in the $^{12}$CO(1→0), $^{12}$CO(2→1), $^{13}$CO(1→0), $^{13}$CO(2→1) lines at the peak position, $\alpha = 0^{\rm h}43^{\rm m}42\overset{\prime\prime}{.}4$, $\delta = -73^\circ 35' 10''$ (1950.0), of the molecular cloud SMCB1#1. The resolution and axis scale are as in Fig. 1

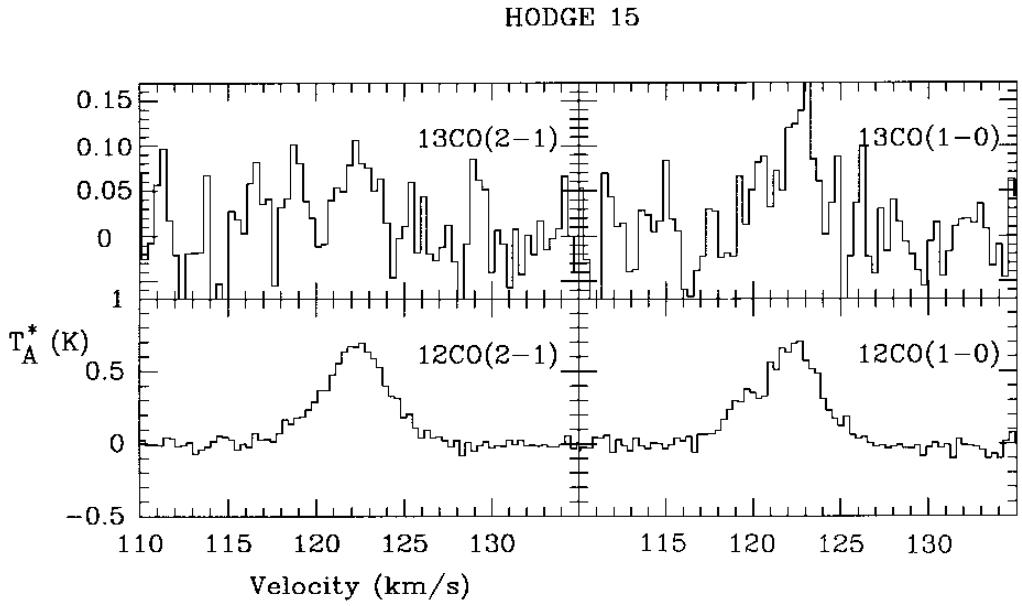


**Fig. 3.** Spectra in the $^{12}$CO(1→0), $^{12}$CO(2→1), $^{13}$CO(1→0), $^{13}$CO(2→1) lines at the peak position, $\alpha = 0^h46^m23\overset{s}{.}0$, $\delta = -73°39'10''$ (1950.0), of the molecular cloud Hodge 15. The resolution and axis scale are as in Fig. 1

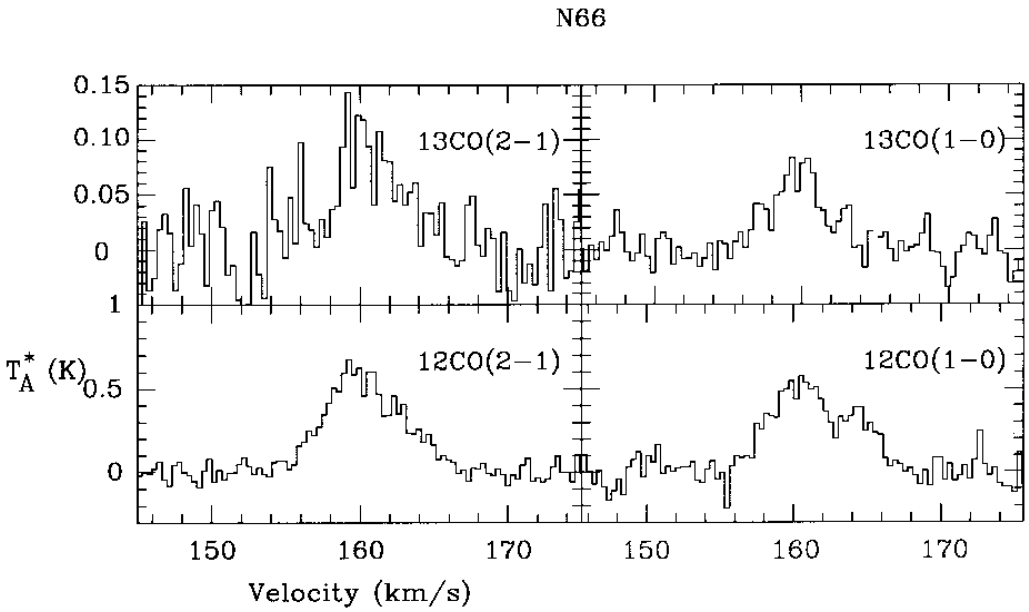


**Fig. 4.** Spectra in the $^{12}$CO(1→0), $^{12}$CO(2→1), $^{13}$CO(1→0), $^{13}$CO(2→1) lines at the peak position, $\alpha = 0^h57^m39\overset{s}{.}7$, $\delta = -72°25'16''$ (1950.0), of the molecular cloud N66. The resolution and axis scale are as in Fig. 1

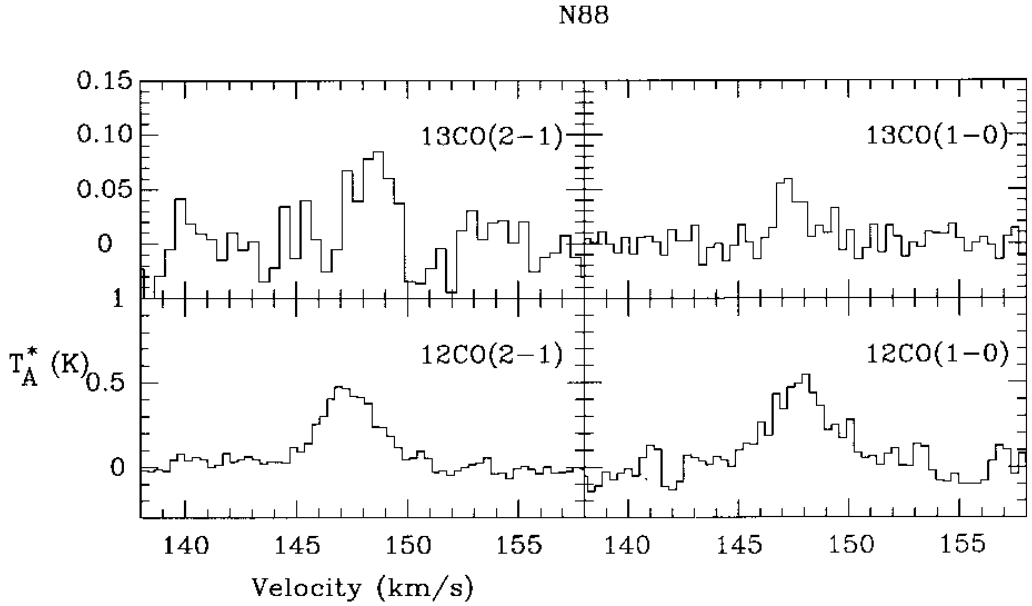


**Fig. 5.** Spectra in the $^{12}$CO(1→0), $^{12}$CO(2→1), $^{13}$CO(1→0), $^{13}$CO(2→1) lines at the peak position, $\alpha = 1^{\rm h}22^{\rm m}54\overset{\rm s}{.}1$, $\delta = -73°24'33''$ (1950.0), of the molecular cloud N88. The resolution and axis scale are as in Fig. 1

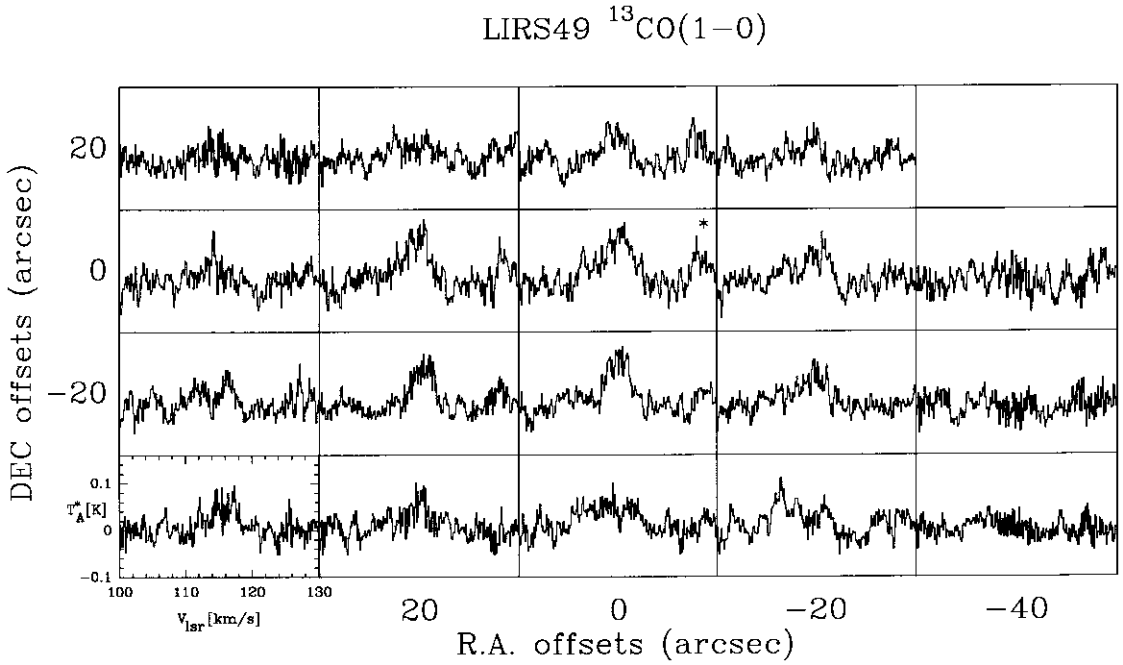


**Fig. 6.** Grids of spectra toward the molecular cloud LIRS 49. The center position (0,0) of the maps is at $\alpha = 0^{\rm h}46^{\rm m}32\overset{\rm s}{.}9$ $\delta = -73°21'\,50''$. The velocity and temperature scales for each box within a panel are the same and indicated in the sample box. Velocity is in $V_{\rm lsr}$ and temperature in $T_{\rm A}^*$. Top panel: $^{12}$CO(1→0) profiles. The resolution is 43″ and the grid step is 20″ × 20″. Middle panel: $^{12}$CO(2→1) profiles. The resolution is 22″ and the grid step is 10″ × 10″. Bottom panel: $^{13}$CO(1→0) profiles. The resolution is 43″ and the grid step is 20″ × 20″

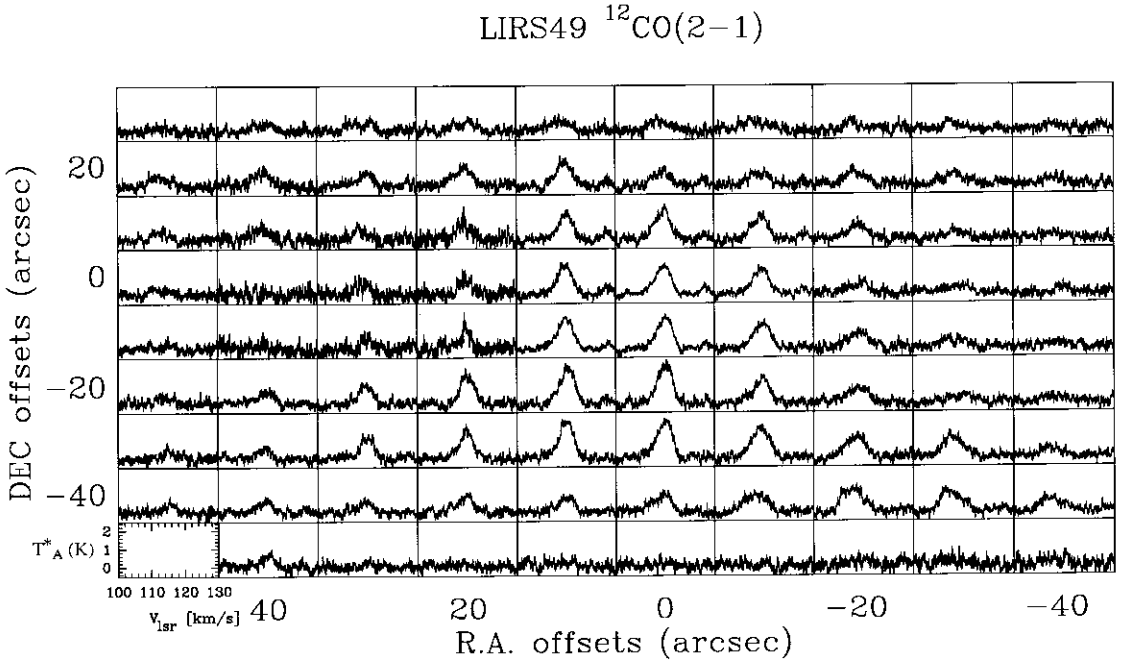


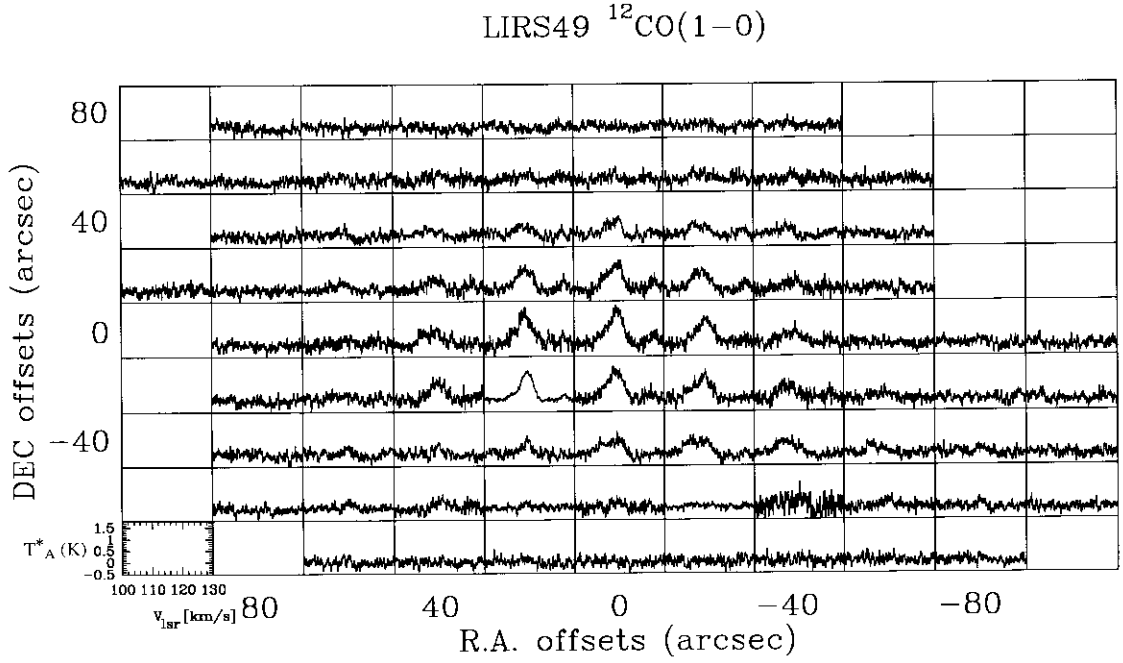


**Fig. 6.** continued

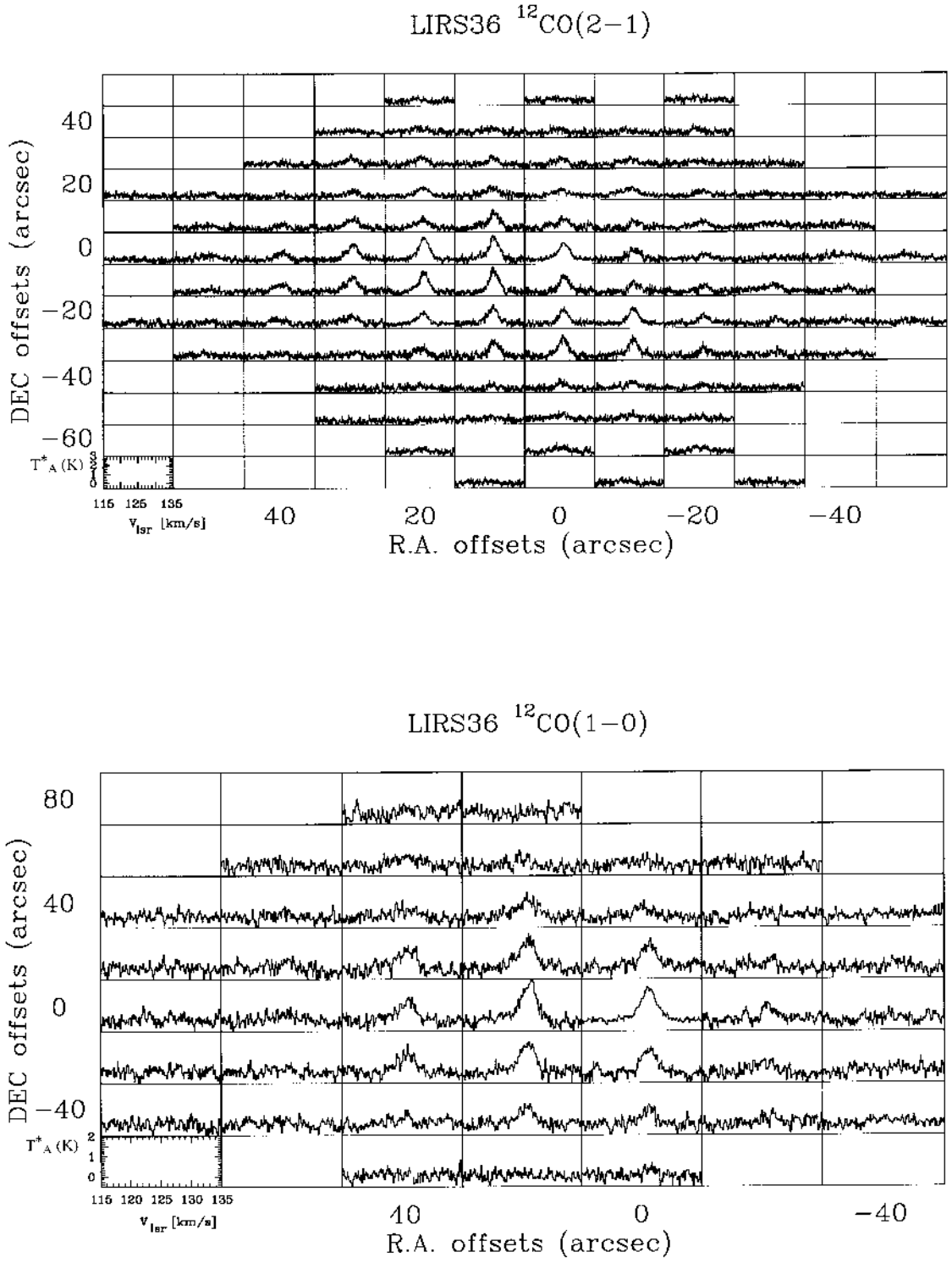


**Fig. 7.** Grids of spectra toward the molecular cloud LIRS 36. The center position (0,0) of the maps is at $\alpha = 0^{\rm h}44^{\rm m}47\overset{\rm s}{.}0$ $\delta = -73^\circ 22' 29''$. Spatial resolution, grid step and axis scales are as in Fig. 6. Note that the peak position in the $^{12}$CO(1→0) line is at the (20″, 0″)offset position. Top panel: $^{12}$CO(1→0) profiles. Bottom panel: $^{12}$CO(2→1) profiles

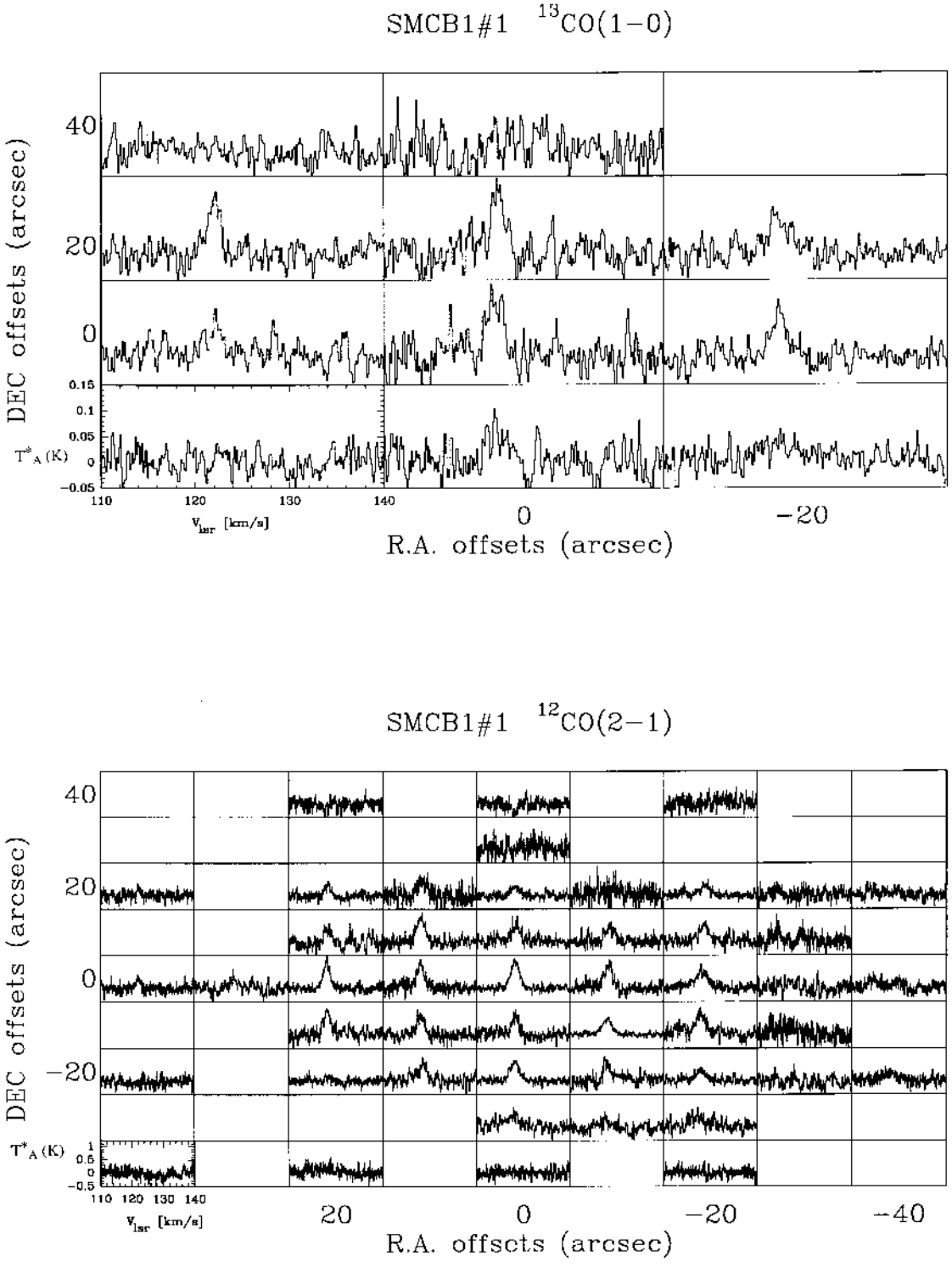


**Fig. 8.** Grids of spectra toward the molecular cloud SMCB1#1. The center position (0,0) of the maps is at $\alpha = 0^h43^m42\overset{s}{.}4$ $\delta = -73°35' 10''$. Spatial resolution, grid step and axis scales are as in Fig. 6. Top panel: $^{12}$CO(1→0) profiles. Middle panel: $^{12}$CO(2→1) profiles. Bottom panel: $^{13}$CO(1→0) profiles

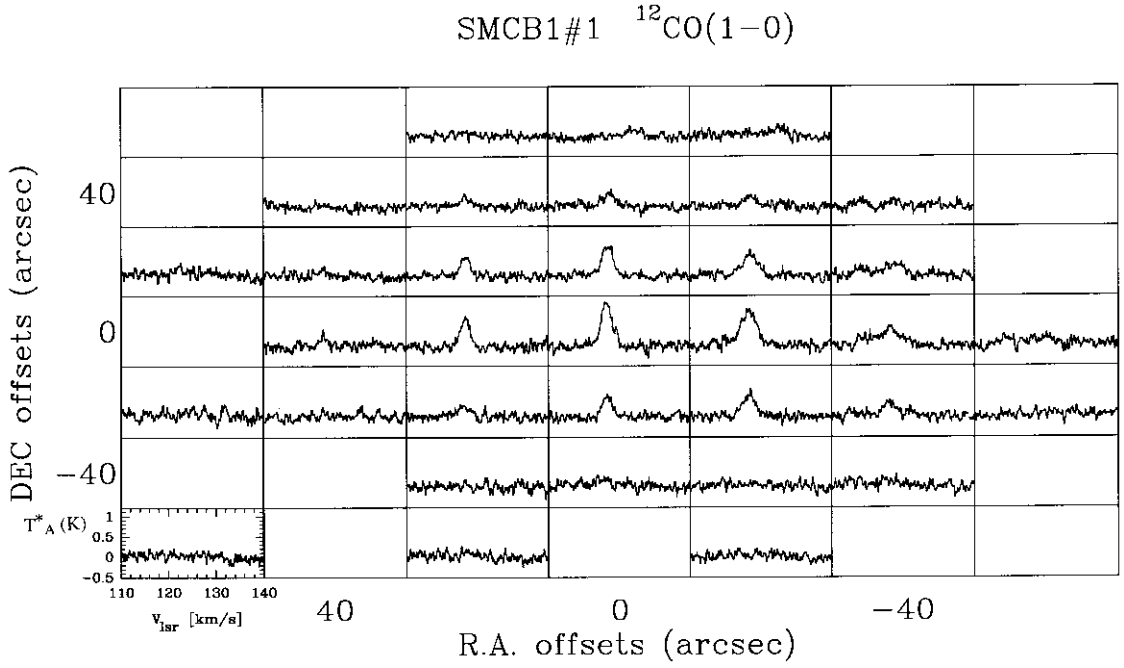


**Fig. 8.** continued

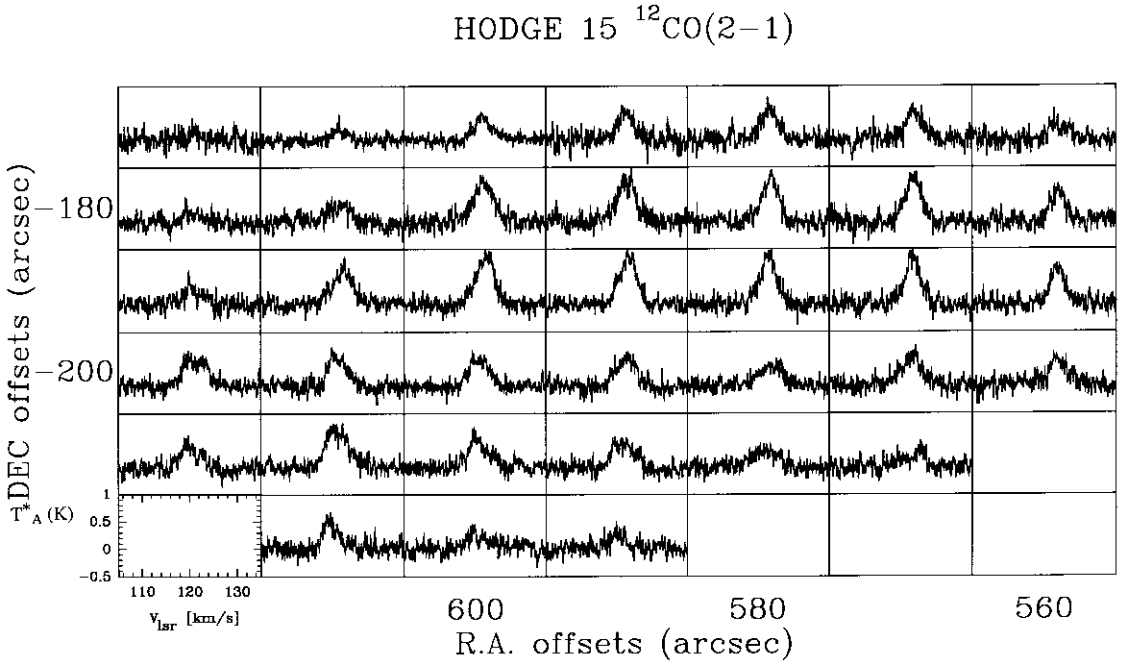


**Fig. 9.** Grids of spectra toward the molecular cloud Hodge 15. The center position (0,0) of the maps is at $\alpha = 0^{\rm h}44^{\rm m}06\overset{\rm s}{.}0$ $\delta = -73^\circ 36' 10''$. Spatial resolution, grid step and scales as for Fig. 6. Note that the peak position in the $^{12}$CO(1→0) line is at the (580″, −180″) offset position of the CO map in the SMC-B2 region (Paper III, their Fig. 3) Top panel: $^{12}$CO(1→0) profiles. Bottom panel: $^{12}$CO(2→1) profiles

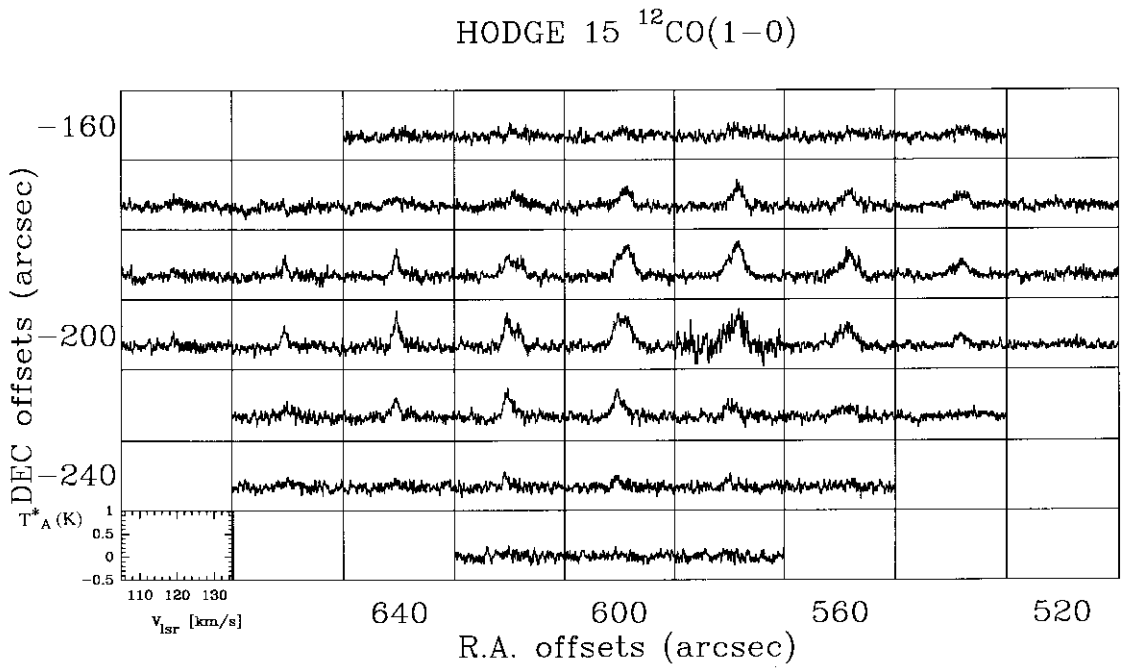


**Fig. 9.** continued

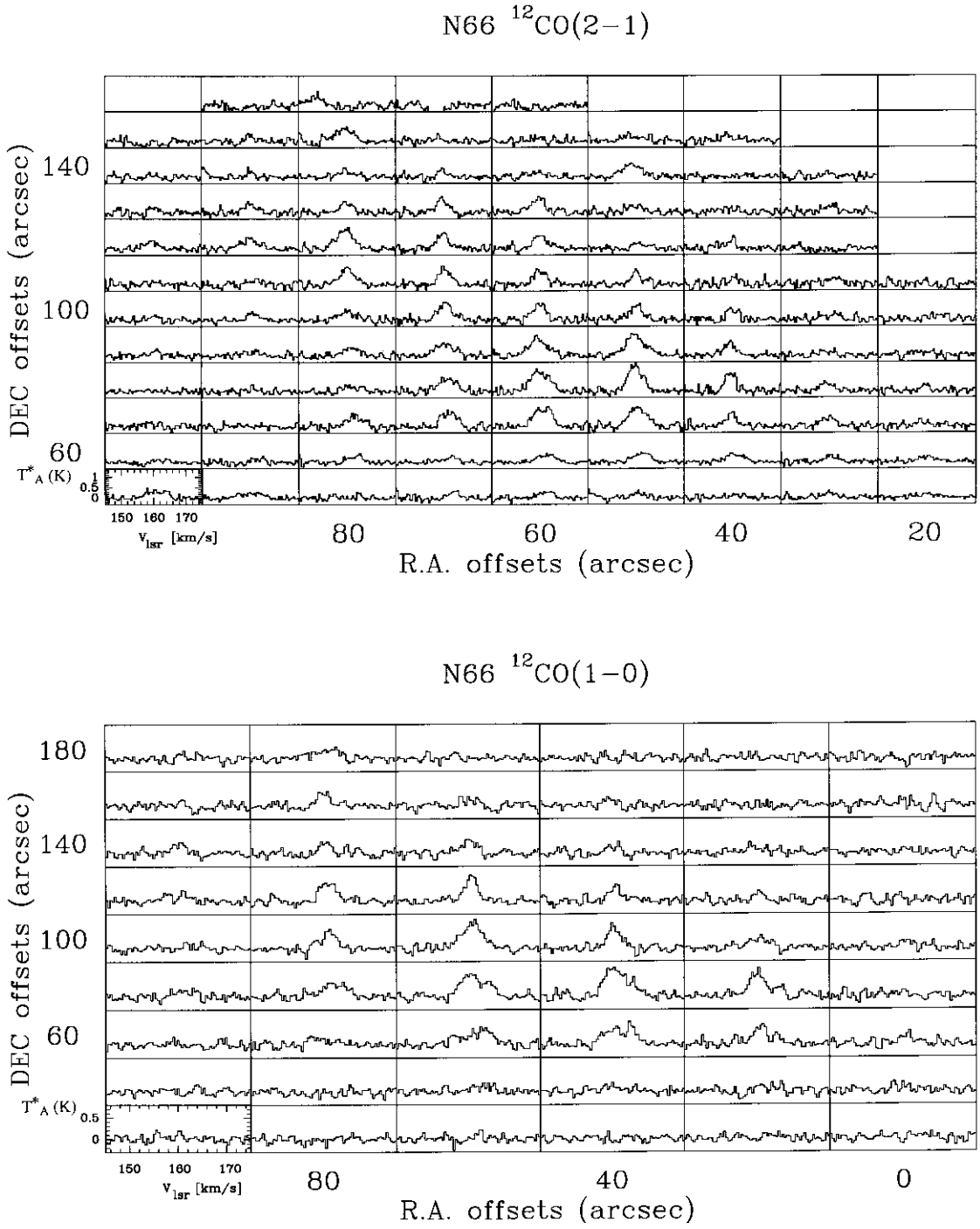


**Fig. 10.** Grids of spectra toward the molecular cloud N66. The center position (0,0) of the maps is at $\alpha = 0^{\rm h}57^{\rm m}26\overset{\rm s}{.}5$ $\delta = -72^\circ 26' 36''$. Spatial resolution, grid step and scales as for Fig. 6. Note that the peak position in the $^{12}$CO(1→0) line is at the (60″, 80″) offset position. Top panel: $^{12}$CO(1→0) profiles. Bottom panel: $^{12}$CO(1→1) profiles

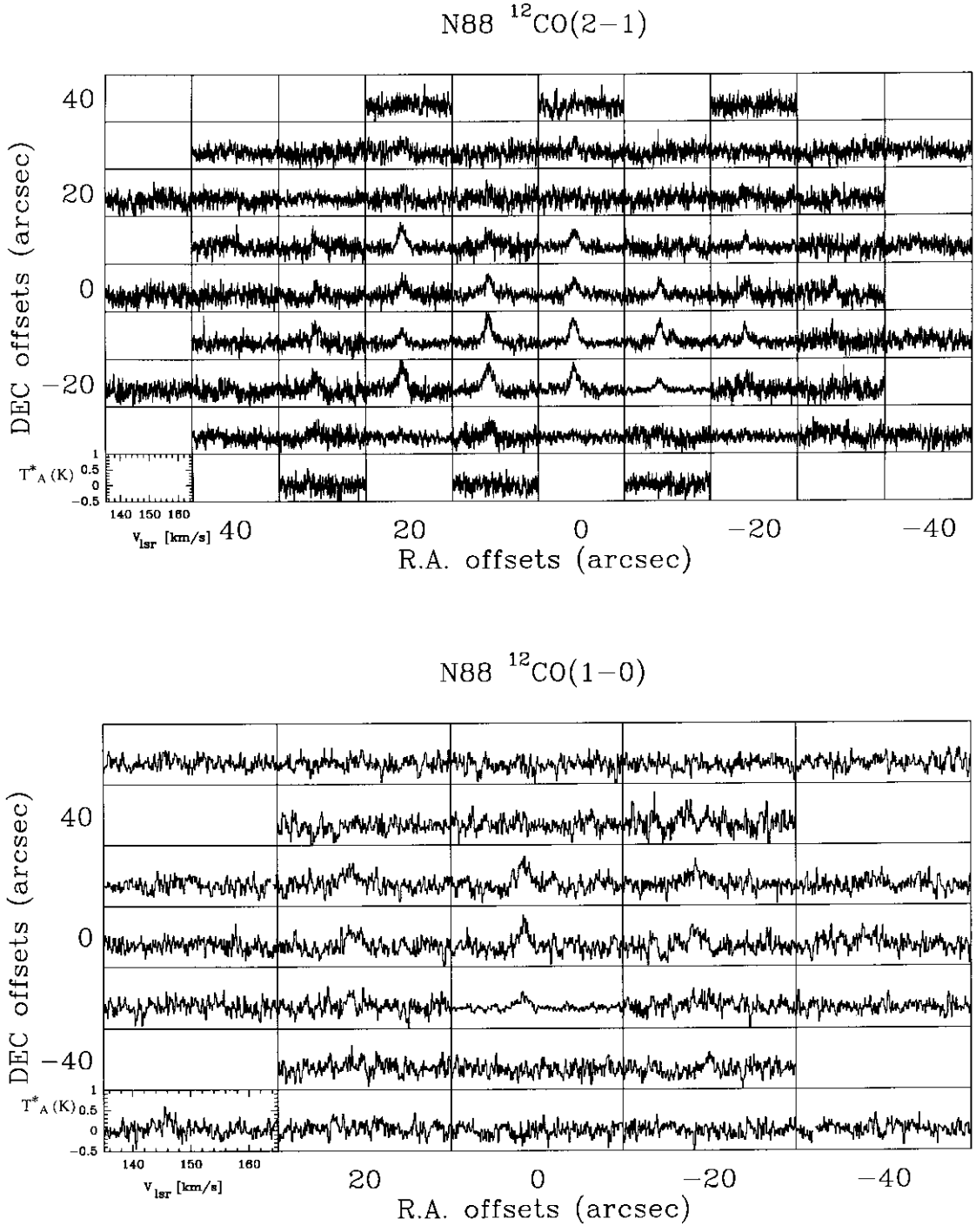


**Fig. 11.** Grids of spectra toward the molecular cloud N88. The center position (0,0) of the maps is at $\alpha = 1^{\rm h}22^{\rm m}54\overset{\rm s}{.}1$, $\delta = -73^\circ 24' 33''$. Spatial resolution, grid step and scales as for Fig. 6. Top panel: $^{12}$CO(1→0) profiles. Bottom panel: $^{12}$CO(2→1) profiles